Dual-spacecraft observation of large-scale magnetic flux ropes in the Martian ionosphere

D. D. Morgan,[1] D. A. Gurnett,[1] F. Akalin,[1] D. A. Brain,[2] J. S. Leisner,[1] F. Duru,[1] R. A. Frahm,[3] and J. D. Winningham[3]

Received 19 September 2010; revised 18 November 2010; accepted 14 December 2010; published 24 February 2011.

[1] We here report the first dual-spacecraft detection of planetary flux ropes in the ionosphere of Mars. The Mars Advanced Radar for Subsurface and Ionosphere Sounding (MARSIS), on board Mars Express, can measure the magnetic field magnitude near the spacecraft. Typically, these measurements track the known crustal magnetic field strength very well; however, occasionally, MARSIS detects transient, intense magnetic fields that deviate significantly from the known crustal fields. Two such magnetic field enhancements occur in near-coincidence with flux rope detections by the Mars Global Surveyor Magnetometer and Electron Reflectometer, which provides vector magnetic field measurements, allowing us to clearly identify the enhancements as flux ropes. The flux ropes detected are quasi-stable for at least a half hour, have peak magnetic field strengths of ~50 and 90 nT, and are ~650–700 km in diameter. Both occur downstream of the region of strong crustal fields. In addition, MARSIS has detected 13 other magnetic enhancements over a 5 year period, which we infer to be flux ropes. These structures have peak field strengths up to 130 nT and measured horizontal dimensions of several hundred to over a thousand kilometers. They are clustered around the intense crustal fields in the southern hemisphere of Mars. The large spatial scale of these flux ropes distinguishes them from small-scale flux ropes, with diameters of tens of kilometers, that have been seen in the ionospheres of Venus and Mars. These large-scale flux ropes are believed to be caused by solar wind stretching and shearing of the Martian crustal fields.

Citation: Morgan, D. D., D. A. Gurnett, F. Akalin, D. A. Brain, J. S. Leisner, F. Duru, R. A. Frahm, and J. D. Winningham (2011), Dual-spacecraft observation of large-scale magnetic flux ropes in the Martian ionosphere, *J. Geophys. Res.*, *116*, A02319, doi:10.1029/2010JA016134.

1. Introduction

[2] In this paper we report the first dual-spacecraft detection of magnetic flux ropes in the ionosphere of Mars. These observations were accomplished on two separate occasions using nearly coincident magnetic field measurements from the Mars Advanced Radar for Subsurface and Ionosphere Sounding (MARSIS) on board the Mars Express (MEX) spacecraft and from the Magnetometer and Electron Reflectometer (MAG/ER) on board the Mars Global Surveyor (MGS) spacecraft. The use of the three-axis magnetometer on MGS allows us to positively identify these two magnetic enhancements as magnetic flux ropes. In addition, we report another 13 similar magnetic field enhancements, observed by MARSIS over a 5 year period, that we believe to be flux ropes. All of these events were observed near the strong crustal field structures in the southern hemisphere of Mars. We will argue that these flux ropes are produced by solar wind stretching and shearing of the crustal magnetic fields containing ionospheric plasma.

[3] The first spacecraft observation of planetary flux ropes at a planet other than Earth was at Venus by *Russell and Elphic* [1979], who defined them as bundles of twisted magnetic field lines that cylindrically wrap about a central axis and contain ionospheric plasma. The field becomes progressively stronger and more axial toward the center. In some cases, the magnetic tension completely dominates all other forces, in which case the plasma pressure gradient is negligible and the magnetic configuration is said to be "force free" [*Priest*, 1990]. Flux ropes are often but not always force free [*Cravens et al.*, 1997]. It is believed that flux ropes can exist along a continuum of deviation from the force free state [*Elphic et al.*, 1980].

[4] Flux ropes are a well-known class of magnetic field structure seen throughout the solar system. In addition to Venus, flux ropes have been observed at the Sun in the form of coronal loops [*Browning*, 1990], in the interstellar medium

[1]Department of Physics and Astronomy, University of Iowa, Iowa City, Iowa, USA.
[2]Space Physics Research Group, Space Sciences Laboratory, University of California, Berkeley, California, USA.
[3]Southwest Research Institute, San Antonio, Texas, USA.

0148-0227/11/2010JA016134

in the form of magnetic clouds [*Lepping et al.*, 1990], and at Earth [*Hesse and Kivelson*, 1998; *Slavin et al.*, 2003] often in association with substorms [*Hones et al.*, 1984a, 1984b]. Most recently, flux ropes have been detected at Mercury by *Slavin et al.* [2009] and Saturn's moon Titan by *Wei et al.* [2010].

[5] Flux ropes at Mars were first reported by *Cloutier et al.* [1999]. A survey by *Vignes et al.* [2004] found an occurrence rate of about 5% of MGS orbits as opposed to 70% detection at Venus by the Pioneer Venus Orbiter [*Elphic and Russell*, 1983]. *Vignes et al.* [2004] also noted that the frequency of occurrence increases with decreasing altitude. These studies showed that the flux ropes detected at Mars were virtually identical to those seen at Venus, except that the peak field strengths ran as high as 60 nT at Venus and only 20 nT at Mars. This type of flux rope is characterized by a diameter of a few tens of kilometers and by an occurrence distribution where there are no planetary or crustal magnetic fields, e.g., the ionosphere of Venus or the northern hemisphere of Mars. Because of their small diameter, *Russell* [1990] refers to this type of flux rope as "filamentary." More recently, *Eastwood et al.* [2008] reported the first observation of a flux rope clearly associated with reconnection signatures in both the magnetic and particle data from MGS. Since then, *Brain et al.* [2010] have observed hundreds of large-scale flux ropes, with diameters of hundreds of kilometers, occurring near the strong crustal fields of Mars. It is this type of "large-scale" flux rope that is detected by MARSIS and that is the topic of this paper.

[6] This paper has seven sections. Section 2 describes the MARSIS instrument, as well as other instruments used in the study, and discusses how the ionospheric radar sounder can be used to measure ionospheric magnetic field strength. Section 3 discusses a MARSIS observation of a transient, localized magnetic field enhancement. Section 4 contains the comparisons between near-coincident observations between MGS MAG/ER and MARSIS that enable us to identify the MARSIS observations as flux ropes. Section 5 briefly discusses electron data from the MGS Electron Reflectometer data taken simultaneously with the magnetometer data discussed in section 4. In this section we also briefly discuss electron flux observations from Analyzer of Space Plasmas and Energetic Atoms (ASPERA)-3 on MEX. Section 6 shows the results of a survey of magnetic enhancements observed by MARSIS that we identify as flux ropes. Section 7 discusses the interpretation of our observations in light of some modeling results and gives the conclusions of this paper.

2. Description of Instruments and Data

[7] MEX [*Chicarro et al.*, 2004], which is in orbit around Mars, carries a low-frequency radar called Mars Advanced Radar for Subsurface and Ionosphere Sounding (MARSIS) that is designed to probe the ionosphere, surface, and subsurface of Mars. In its ionospheric mode MARSIS operates by applying a 400 V, 91.4 μs, quasi-sinusoidal pulse at a fixed frequency, to the 40 m antenna. After the pulse the instrument is switched to "receive" mode in order to detect the reflected signals. The instrument remains in receive mode for 80 consecutive detection intervals, designated as "time delay" bins, of 91.4 μs each. When the transmission pulse and associated dead-time intervals are taken into account, a complete transmit-receive cycle at a given frequency takes 7.857 ms. The transmitted frequencies are stepped through 160 values from 0.1 to 5.5 MHz. The output of MARSIS in ionospheric mode, therefore, consists of an array of 160 × 80 received spectral densities that requires 1.257 s to collect. When displayed graphically, the array of spectral densities is referred to as an ionogram, a sample of which is shown in Figure 1. An ionogram is collected every 7.543 s. The longitude given here and throughout the paper is west longitude. For further information on the MARSIS instrument, see *Picardi et al.* [2004] and *Jordan et al.* [2009].

[8] The features in Figure 1 labeled "vertical ionospheric echo" and "surface reflection" represent reflections from the ionosphere and the surface of the planet. The other two features, labeled "electron plasma oscillation harmonics" and "electron cyclotron echoes," are the result of interactions between the sounding pulse and the plasma near the spacecraft. The plasma oscillation harmonics are an instrumental response to electron plasma oscillations excited in the plasma near the spacecraft by the sounding pulse. They are scientifically useful [*Duru et al.*, 2008; *Morgan et al.*, 2008] because they give a direct measurement of the plasma frequency and therefore the electron density near the spacecraft. The electron cyclotron echoes are caused by electrons accelerated by the sounding pulse that execute cyclotron orbits in the ambient magnetic field. Once per cyclotron period the electrons return to the vicinity of the spacecraft, where they produce a voltage on the antenna. These echoes occur with a repetition rate equal to the electron cyclotron period and therefore provide a way of measuring the magnetic field strength near the spacecraft. The electron cyclotron echoes were first noted in the MARSIS data and explained by *Gurnett et al.* [2005]. They were further studied by *Akalin et al.* [2010], who first noted the occurrence of strong localized noncrustal magnetic field enhancements.

[9] Because the time interval between echoes is the electron cyclotron period, it is a simple matter to calculate the local magnetic field strength using

$$f_c = \frac{1}{T_c} = \frac{eB}{2\pi m}, \tag{1}$$

where f_c is the local electron cyclotron frequency, T_c the corresponding electron cyclotron period, e the electron charge, B the local magnetic field strength, and m the electron mass. Equation (1) can then be solved to give the magnetic field strength

$$|B| \ [\mathrm{nT}] = \frac{1000}{28 T_c \ [\mathrm{ms}]}. \tag{2}$$

[10] *Gurnett et al.* [2005] and *Akalin et al.* [2010] have compared magnetic field strengths derived by this method with the crustal field model of *Cain et al.* [2003] (hereinafter referred to as the "Cain model"), which in turn is derived from MGS spacecraft magnetometer data. The strong correspondence that they find between MARSIS data and the Cain model confirms that the electron cyclotron echoes are a direct measure of the magnetic field magnitude at the

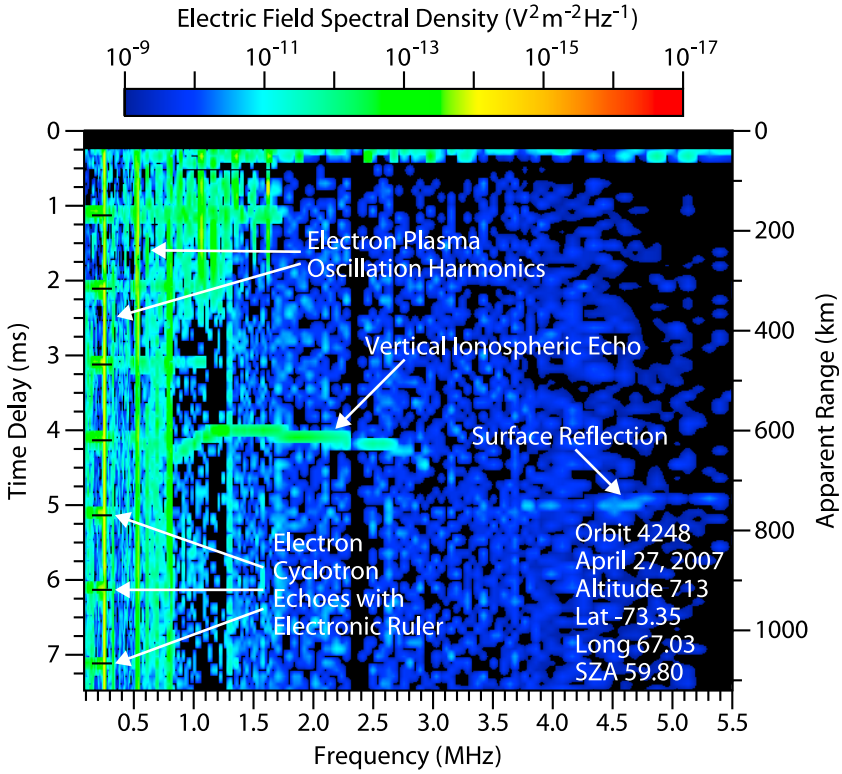

Figure 1. A sample Mars Advanced Radar for Subsurface and Ionosphere Sounding (MARSIS) ionospheric sounder ionogram showing four principal measurements: the electron plasma oscillation harmonics (upper left), the vertical ionospheric echo (center left),the surface reflection (center right), and the electron cyclotron echoes (bottom left). The ionogram is a representation of received spectral density as a function of sounding frequency and time delay from the sounding pulse. The longitude given here and throughout the paper is west longitude.

spacecraft. While the Cain model is based primarily on nightside data from the MGS magnetometer (with a component of low-altitude dayside data), the MARSIS magnetic field studies have focused on data from the dayside of Mars. Although the MARSIS-derived magnetic field magnitudes track the corresponding values from the Cain model very well, the MARSIS magnitudes are typically greater than those from the Cain model over regions of significant crustal fields. This difference is due to the addition of the compressed and draped solar wind magnetic field [see *Brain et al.*, 2003]. The solar wind magnetic field, therefore, can, in general, effect the ionosphere of Mars. What we shall see in section 3 is that the difference between the measured and model fields can take the form of isolated regions of strong, transient magnetic field.

[11] In this work we also use data from MEX ASPERA-3 [*Barabash et al.*, 2004] and MGS MAG/ER [*Acuña et al.*, 2001; *Mitchell et al.*, 2001]. The electron spectrometer (ELS) of ASPERA-3 has an energy range of 0.5 eV to 20 keV per charge with in 127 logarithmically spaced channels with resolution $\Delta E/E$ = 0.08. A full sweep in energy takes 4 s. Spacecraft charging of approximately −5 V in the Martian ionosphere prevents us from seeing the cold component of electrons. In the solar wind or magnetosheath, the spacecraft charges to about +8 V, which should allow the lowest energy electrons to be seen. The intrinsic angular field of view is 4° × 360° in 16 azimuthally spaced sensors.

[12] The Ion Mass Analyzer (IMA) has an energy range of 10 eV to 30 keV per charge measured in 96 energy channels. Up until May 2007 the energy channels were spaced logarithmically with $\Delta E/E = 0.07$. After that date the coverage of ions of energy less than 50 eV was optimized by reprogramming the spacing to be linear and changing its angular accumulation. Because our coincidence measurements, to be given in detail in section 4, were taken before that date, the IMA had difficulty in detecting ionospheric ions.

[13] The MGS MAG/ER instrument is described by *Mitchell et al.* [2001] for the electron reflectometer and by *Acuña et al.* [2001] for the magnetometer. The electron reflectometer spans a field of view of 360° × 14° with energy coverage from 10 eV to 20 keV with resolution $\Delta E/E = 0.25$ full width at half maximum. The angular resolution is 22.5°. Because MGS was a nonspinning spacecraft, acquisition of a complete pitch angle distribution is problematic. The MGS magnetometer provides three-dimensional magnetic field measurements up to $\approx 6.6 \times 10^4$ nT with 12 bit digital resolution. It is accurate to 0.5–1.0 nT [*Acuña et al.*, 2001], much smaller than the structures under study in this work.

3. Observations of Transient Magnetic Field Enhancements

[14] In the studies by *Gurnett et al.* [2005] and *Akalin et al.* [2010], MARSIS measurements of the magnetic field

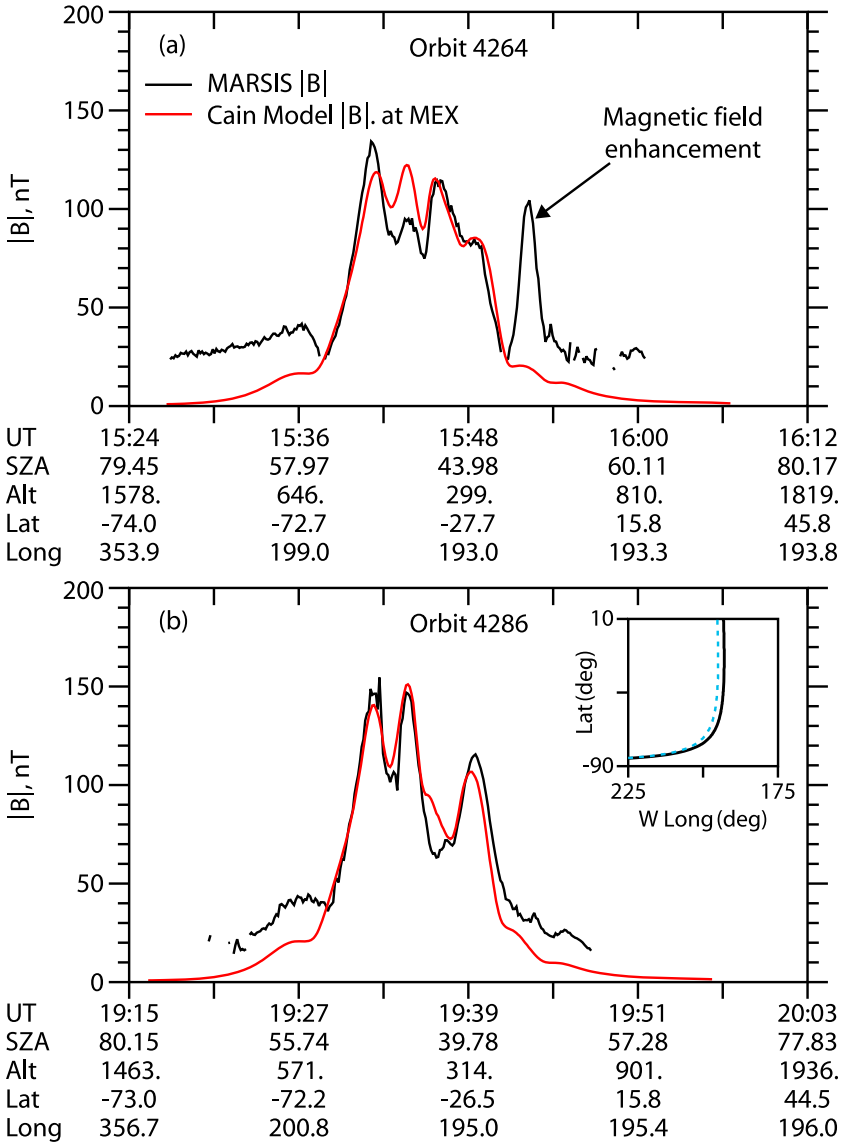

Figure 2. Comparison of the magnetic field measured by MARSIS with the crustal magnetic field strength computed from the Cain model at the position of the spacecraft. The vertical axis represents the magnetic field strength; the horizontal axis represents time with accompanying ephemeris quantities. Black curves represent the magnetic field strength measured by MARSIS. Red curves represent the Cain model value of the crustal magnetic field strength at the spacecraft. (a) Orbit 4264, which includes a non-crustal enhancement between ~1549 and 1554 UT. (b) Orbit 4286, whose ground track is nearly identical to that of orbit 4264. The inset in Figure 2b shows the two ground tracks: orbit 4264 in black and orbit 4286 in blue-green, approximately aligned in latitude. Note that orbit 4286 does not show any noncrustal enhancement like that seen in orbit 4264 for latitudes between −25° and 15°.

are compared to the Cain model, and the correlation between the measurements and the model are studied. *Akalin et al.* [2010] observed that occasionally the magnetic field observed by MARSIS is strongly enhanced in localized regions where the Cain model does not predict strong crustal fields. An example of such an event is shown in Figure 2.

[15] A particularly strong noncrustal magnetic field enhancement detected on Mars Express orbit 4264, 1 May 2007, is shown in Figure 2a. Through most of the orbit, the magnetic field strength measured by MARSIS, shown in black, closely tracks the crustal field from the Cain model, shown in red; however, between 1550 and 1554 UT, the MARSIS magnetic field shows a large deviation from the crustal field. Figure 2b shows the same quantities from orbit 4286, 7 May 2007, which followed a near-identical path. Figures 2a and 2b are approximately aligned in latitude. The inset in Figure 2b shows the two ground paths, orbit 4264 in black, orbit 4286 in blue-green. It can be seen that there is no deviation from the crustal field in orbit 4286 comparable

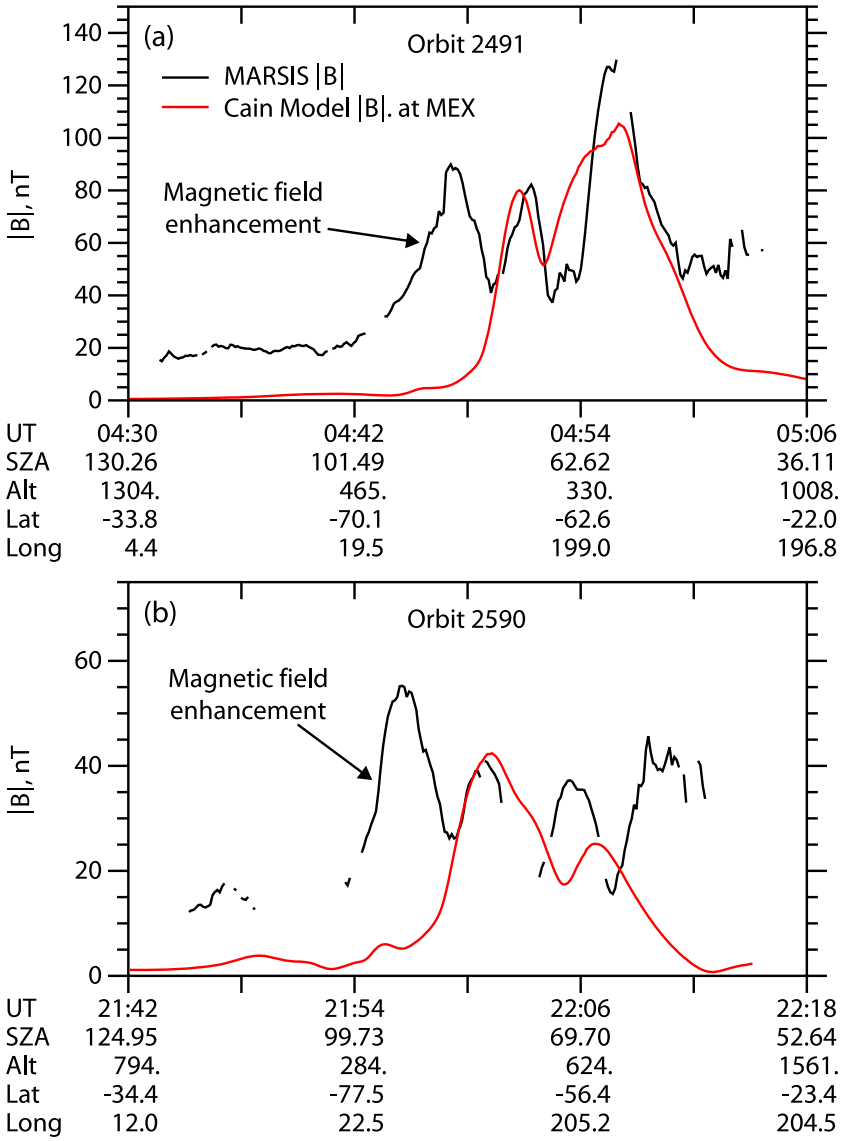

Figure 3. Two magnetic field enhancements on orbits (a) 2491 and (b) 2590. MARSIS magnetic field strength is shown in black, crustal field strength from the Cain model is shown in red.

to that in orbit 4264. The magnetic field enhancement of orbit 4264 is therefore a transient event.

4. Comparison of MARSIS Magnetic Field Enhancements With Near-Coincident MGS Magnetometer Observations

[16] Two well-defined noncrustal magnetic field enhancements observed by MARSIS on orbits 2491 and 2590 are shown in Figures 3a and 3b. As in Figure 2, the black curves represent the magnetic field strength as measured by MARSIS, and the red curves represent the Cain model field strength. As with orbit 4264 in Figure 2a, the local magnetic field strength shows an enhancement while the crustal magnetic field computed from the Cain model remains small. These two events are nearly coincident with magnetic enhancements observed by the Magnetometer/Electron Reflectometer (MAG/ER) on board MGS. We now examine these two events in detail.

[17] The MGS magnetometer data corresponding to the magnetic enhancements shown in Figures 3a and 3b are shown in Figures 4a and 4b. In Figures 4a and 4b (top), the magnetic field strength measured by MGS MAG is shown in black, compared with the crustal field strength at the position of MGS from the Cain model, shown in red. The MGS field strength exceeds the crustal field by a large factor between 0510 and 0518 UT in Figure 4a and between 2224 and 2230 UT in Figure 4b. The vertical dashed lines indicate the time of detection of the peak magnetic field strength from MARSIS. In both cases the MGS MAG peak fields follow those of MARSIS by approximately a half hour. The bottom halves of both Figures 4a and 4b show the magnetic field components from MGS in Mars Solar Orbital (MSO) coordinates. (MSO coordinates are defined as follows: x points from the planetary center of mass to the

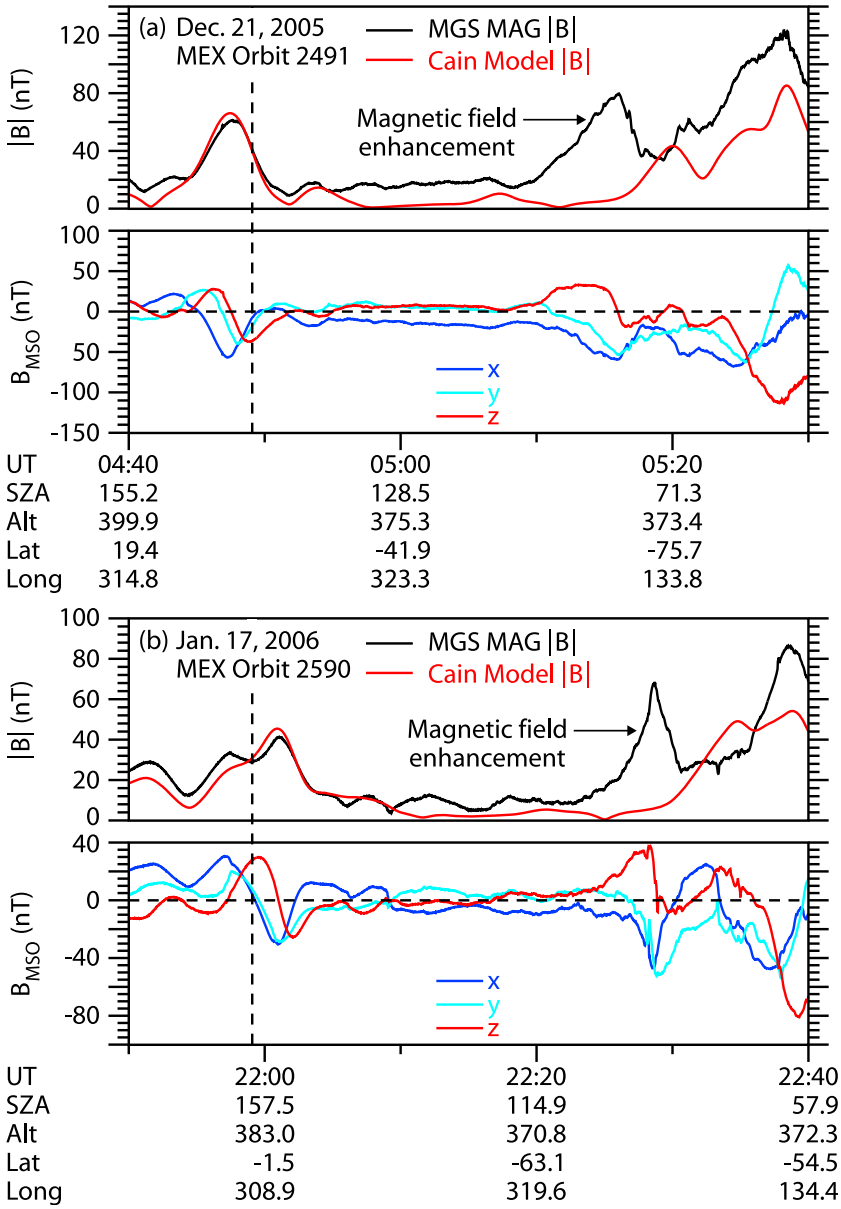

Figure 4. Mars Global Surveyor (MGS) magnetometer observations made in near-coincidence with the MARSIS observations made on Mars Express orbits (a) 2491 and (b) 2590. (top) MGS magnetic field strength in black with the Cain model field strength at the position of the spacecraft in red. (bottom) Three magnetic field components in Mars Solar Orbital coordinates. The vertical dashed line indicates the time of the corresponding MARSIS detection.

Sun, z points normal to the Mars orbital plane, and y completes the right-handed triad [*Acuña et al.*, 2001]. In this reference, MSO coordinates are referred to as Sun-state coordinates.)

[18] Magnetic field strengths measured by MARSIS (red) and MGS MAG/ER (green) are shown as a function of position along the ground tracks of Mars Express and MGS in Figure 5, orbit 2491 (Figure 5a) and orbit 2590 (Figure 5b). The approximate Sun direction for the MARSIS peak magnetic field detection indicates the approximate source direction of the solar wind. Figure 5 shows that the MARSIS and MGS measurements are spatially adjacent as well as nearly simultaneous. Both events are downstream of the strong crustal magnetic fields between 40°S and 85°S and between 150°W and 210°W, with peak magnetic field strengths occurring very close to the Martian south pole.

[19] The MGS magnetometer measures all three components of the magnetic field, allowing us to use minimum variance analysis to determine the evolution of the magnetic field [*Sonnerup and Cahill*, 1968]. The results of this analysis, called a hodogram and shown in Figure 6, show the evolution of the magnetic field analyzed in the axes of maximum, intermediate, and minimum variance, labeled in Figure 6 as B_{MVA1}, B_{MVA2}, and B_{MVA3}. The ordering of the axes can be expressed as a ratio of eigenvalues. In these cases, the eigenvalue ratios are 1:0.417:0.024 and

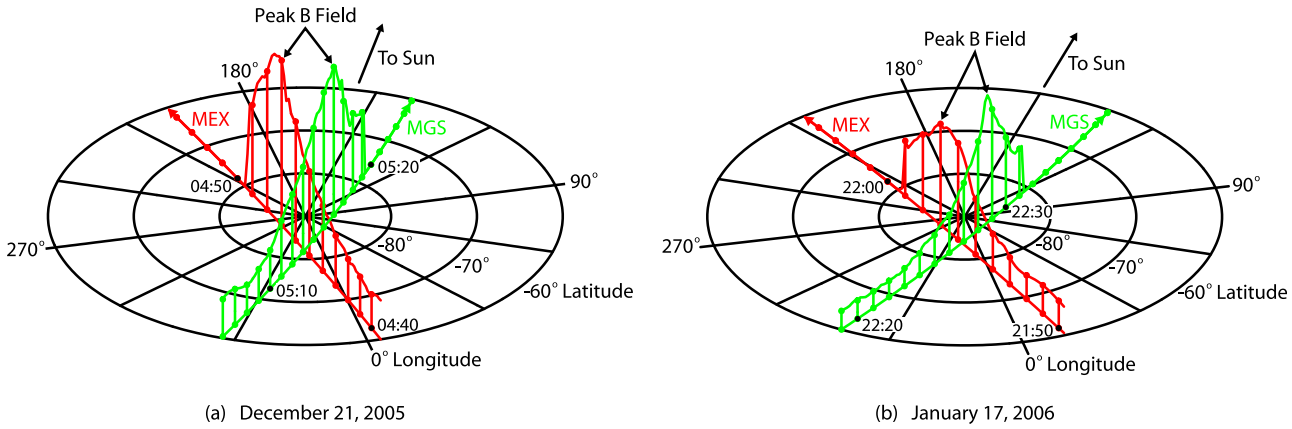

Figure 5. Near-simultaneous observations of a large-scale flux rope by Mars Express and MGS during Mars Express orbits (a) 2491 and (b) 2590. The magnetic field strength is shown as a function of position on the ground track of each spacecraft. Sun direction for the MARSIS detection is shown by an arrow.

1:0.457:0.035, indicating a clear differentiation of the maximum, intermediate, and minimum variance axes for both of these events. The rotation evident in the maximum-intermediate plane (right-hand column of 6) combined with the vertical appearance in the minimum-maximum plane (left-hand column of 6) is characteristic of a magnetic flux rope. The unambiguous identification of the three axes enables us to identify the intermediate axis as, approximately, the axis of the flux rope [*Lepping et al.*, 1990]. This identification is reinforced by the unidirectional variation along the intermediate variance direction. This estimate of the direction of the flux rope axis is shown as a blue arrow in Figures 7a and 7b,

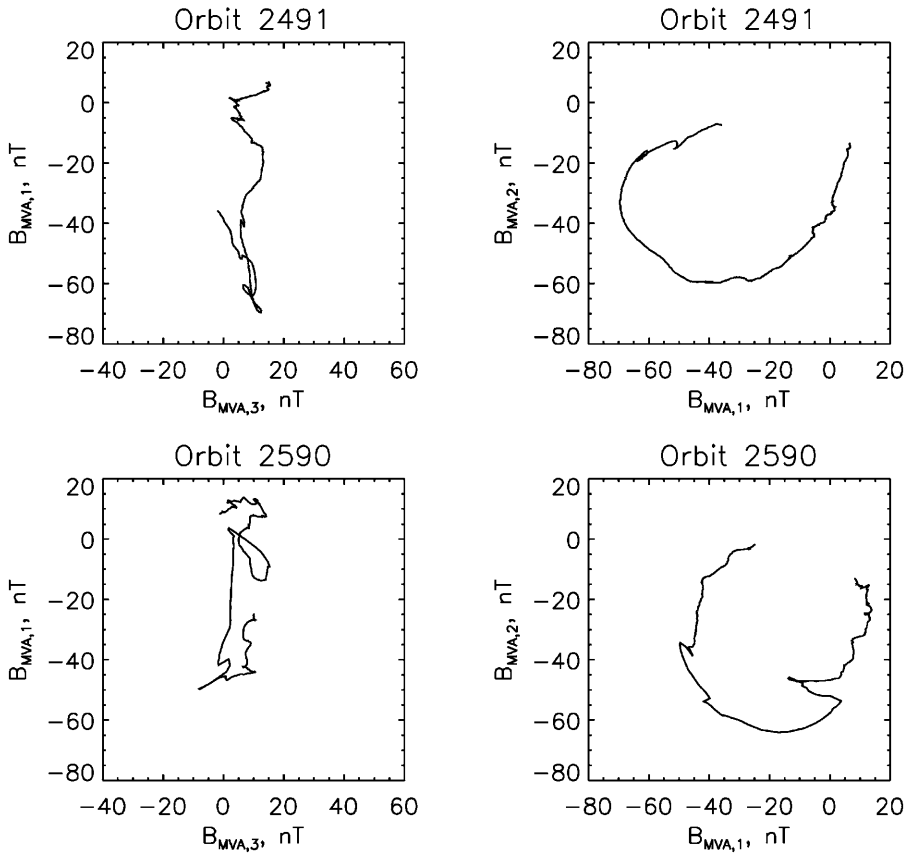

Figure 6. Hodograms for MGS observations of MARSIS magnetic field enhancement on (top) orbit 2491 and (bottom) orbit 2590. Axes labeled MVA1, MVA2, and MVA3 represent the maximum, intermediate, and minimum variance axes, respectively.

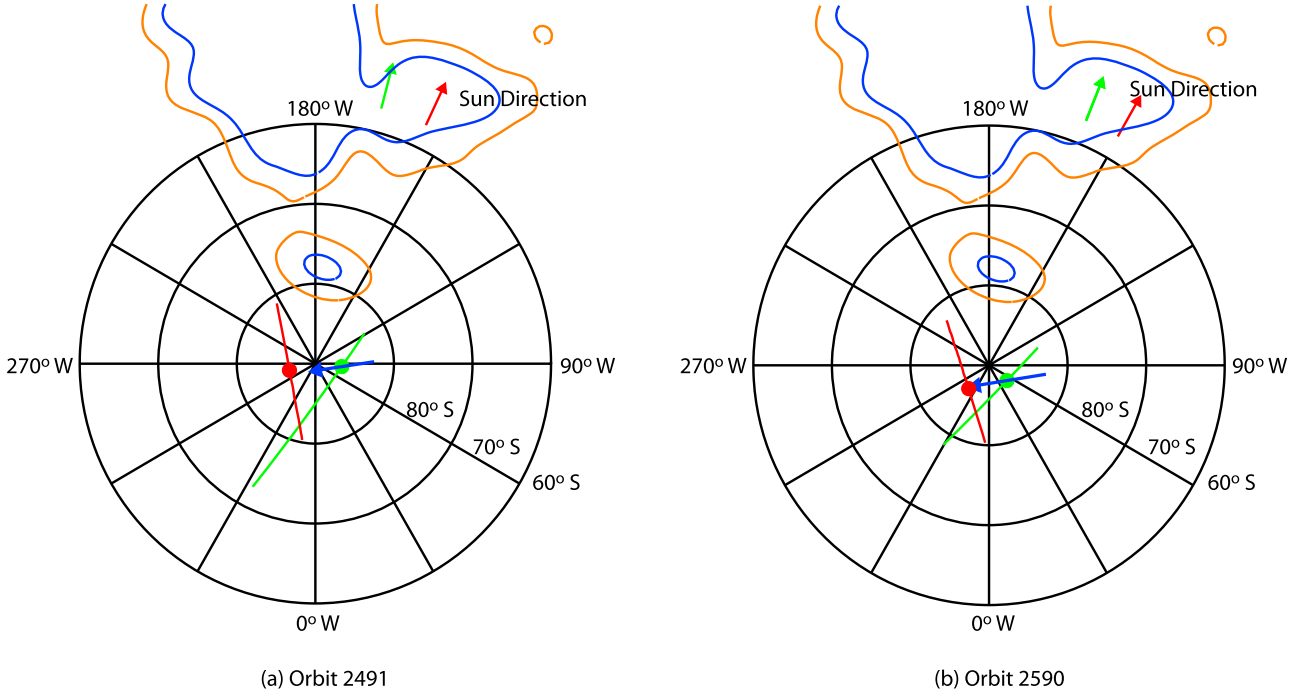

Figure 7. Polar plots showing ground tracks of jointly observed events on Mars Express orbits (a) 2491 and (b) 2590. Ground tracks for MGS are shown in green; those for Mars Express are shown in red. The dot seen midtrack represents the peak magnetic field strength. The flux rope axis directions obtained from minimum variance analysis are indicated by a blue arrow intersecting the MGS ground track at the point of peak field strength. Crustal magnetic field strength contours from the Cain model computed at 400 km altitude are indicated by orange (50 nT) and dark blue (75 nT) curves. The Sun direction for each ground track in corresponding color is given at the outer boundary of each plot. The flux ropes are seen to occur downstream from strong crustal magnetic arcades in the Martian southern hemisphere. The inferred flux rope axis directly connects the peak field strengths of the MGS and MARSIS detections.

which show the ground tracks of the MGS and MARSIS observations with Sun direction and the position of high-field-strength crustal field contours. In both cases, the flux rope axis is oblique to the solar wind direction and the flux rope is observed directly downstream from the crustal magnetic structures. It should be noted that the peak-field-strength positions of the MGS and MARSIS measurements line up along the inferred flux rope axis, implying that the flux rope configuration exists in a quasi steady state over the half hour between measurements. If we assume stationary ionospheric plasma near the terminator, the orientation of the flux rope axis nearly perpendicular to the MARSIS ground tracks for both events allows us to estimate the diameter of the flux rope at 650–700 km.

5. Electron Signatures Seen by the MGS Electron Reflectometer and MEX ASPERA-3 ELS

[20] Next we discuss electron distributions observed concurrently with the magnetic field observations. Magnetic field and particle data from MGS MAG/ER are shown in Figure 8 (left) for the orbit 2491 event and Figure 8 (right), for the orbit 2590 event. The timescale is expanded to show only the times immediately surrounding the two flux ropes. Figures 8a, 8b, 8e, and 8f repeat the MGS MAG data from Figures 4a and 4b with expanded timescales. Figures 8c and 8g show the corresponding omnidirectional spectrograms of the electron differential energy flux. In both Figures 8c and 8g, we observe that the electron differential energy flux between 10 and 10^3 eV is depressed near the beginning and end of MGS's transit of the flux rope. In the interior of the flux rope, the flux rises almost to its level outside the flux rope and then falls off again. Figures 8d and 8h show corresponding spectrograms of pitch angle for the 115 eV energy channel (an attenuator possibly affects lower-energy channels). In both events, the period of depressed electron flux as MGS enters the flux rope coincides with intense field-aligned electrons and with a perpendicular population of shorter duration. As the peak in magnetic field strength is approached, the electron population becomes isotropic and remains so for the duration of the flux rope encounter. The anisotropy is not symmetric with respect to ingress and egress from the flux rope; it is only observed on the incoming ramp. These pitch angle distributions are similar to those in the main case discussed by *Brain et al.* [2010] except that those authors detect field-aligned electrons both before and after closest approach to the core of the flux rope.

[21] We have examined electron and ion distributions from ASPERA-3, the plasma instrument on board Mars

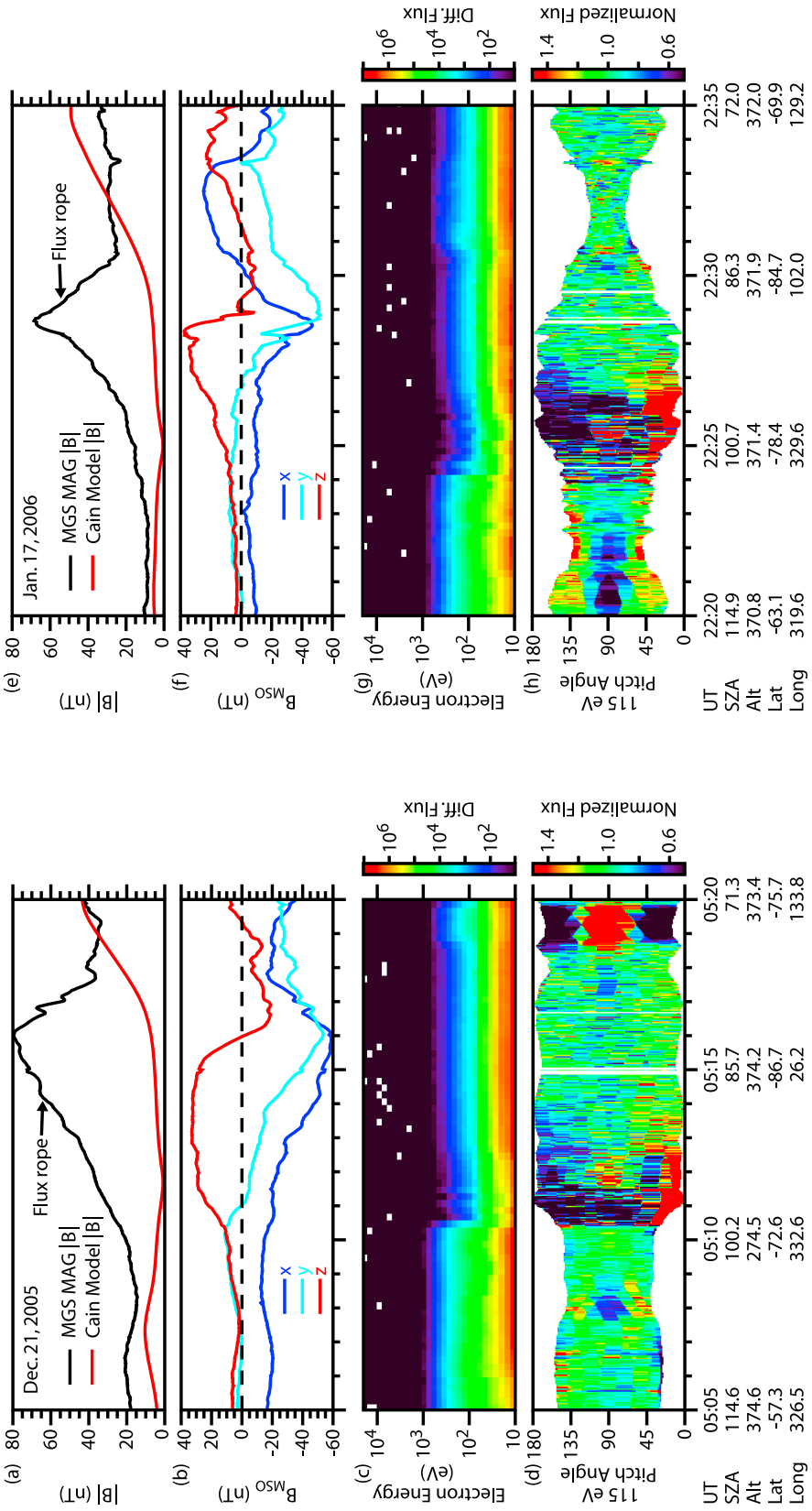

Figure 8. Magnetic enhancements detected by MGS Magnetometer and Electron Reflectometer approximately a half hour after detections by MARSIS on orbits (left) 2491 and (right) 2590. The timescales are expanded around the MGS flux rope events. Figures 8a, 8b, 8e, and 8f show the same information as Figure 4 with the timescale expanded. Figures 8c and 8g are spectrograms of electron differential energy flux. Figures 8d and 8h are spectrograms of the normalized flux with respect to pitch angle at a constant electron energy of 115 eV.

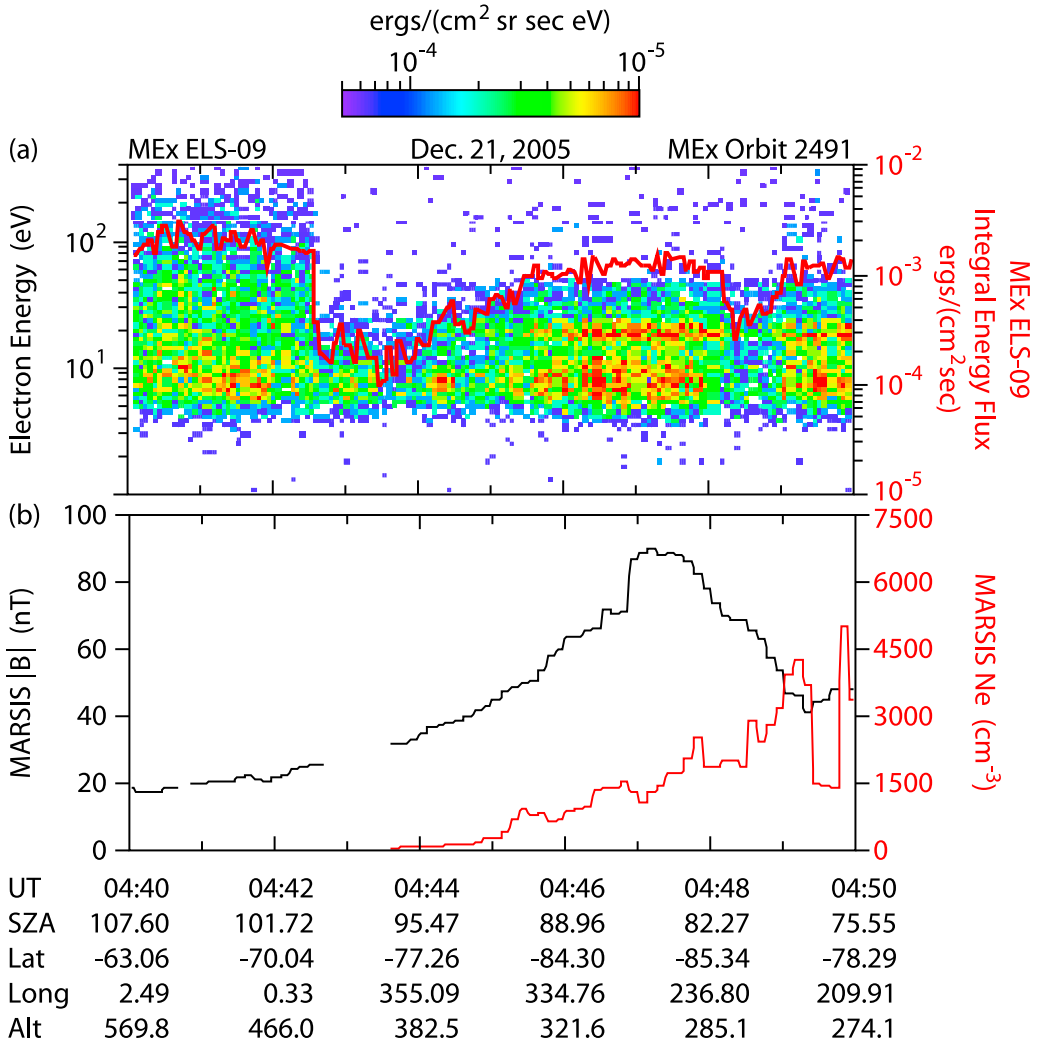

Figure 9. (a) Analyzer of Space Plasmas and Energetic Atoms-3 electron spectrometer differential energy flux, anode 9, for the time surrounding the MARSIS flux rope detection. The red line is the integrated electron flux. (b) MARSIS magnetic field strength (black) and electron density (red) during this flux rope detection.

Express, at the time of the large-scale flux rope detection for the event of orbit 2491 and three other similar magnetic field enhancements observed by MARSIS. There were no obvious changes in the ion energy distributions as measured by IMA; however, note that linear spacing of the lowest energy range had not been implemented at that time, impairing detection of ionospheric electrons [*Lundin et al.*, 2008]. The observed flux decreases in MGS differential energy flux shown in Figure 8c are confirmed by ASPERA-3 ELS data, shown in Figure 9a as a spectrogram of differential energy flux, measured by anode 9, of the ELS, as a function of time. (Anode 9 appears to be most representative of the anodes uncontaminated by spacecraft photoelectrons.) The occurrence of the discrete photoelectron band at about 20 eV indicates that the plasma detected by ELS is wholly ionospheric during detection of the flux rope. Figure 9b shows the MARSIS magnetic field strength and electron density. Similar ASPERA-3 ELS measurements for Orbit 2590 are similar to those for Orbit 2491 and are not shown here. Observed decreases in ionospheric electron flux at about 0443:30 and 0448:30 UT are not accounted for by the change in altitude and solar zenith angle as tabulated below Figure 9b. These decreases are therefore most easily explained as due to ionospheric electron distributions that are elongated along the rotating magnetic field combined with sampling that does not cover 4π steradians. We believe that when such dropouts are observed, they corroborate the torsional structure of the detected magnetic field.

6. Other Observations of Flux Ropes by MARSIS

[22] In a survey of 1939 orbits between orbits 1830 and 6698 (19 June 2005 to 22 March 2009), 39 candidates for a noncrustal magnetic field enhancement were identified. These events were selected visually from plots similar to the two parts of Figure 3. Approximate time boundaries of the events were also selected visually. Enhancements occurring only over strong crustal field structures were not considered; however, enhancements adjacent to or only partially over strong crustal fields were allowed. Indeed, all cases were

found to occur fairly close to strong crustal field structures, centered in the southern hemisphere.

[23] To cull out doubtful cases, we required that the magnetic field strength drop from the peak value by a factor of the square root of two on both sides of the peak. This constraint is necessarily weak because many plausible cases are adjacent to strong crustal arcades, which can truncate the perceived edge of the flux rope. However, if the magnetic field outside the $1/\sqrt{2}$ boundaries on either side had a median above $B_{\mathrm{Peak}}/\sqrt{2}$, the boundary was considered to be unclear and the case excluded. This procedure left us with 15 cases to analyze, including those discussed in sections 3 and 4.

[24] The spacecraft local magnetic field strength and maximum-normalized electron density for the 15 selected flux ropes are plotted as a function of time in Figure 10. The traces for both measurements are centered on the peak magnetic field time. The measurements are given in ascending order of altitude of the magnetic field strength peak, with Figure 10a giving the bottom five passes in altitude, Figure 10b the middle five, and Figure 10c the top five. The MARSIS magnetic field strengths are plotted in black. The electron densities measured by MARSIS, normalized so that the maximum value is one, are overplotted in red. Finally, the MARSIS electron density corrected using a simple model based on the work of *Duru et al.* [2008] and normalized so that the maximum value is 1 is plotted in blue. We note that, while some flux ropes appear to have a decrease in density correlated with the peak magnetic field, it is not a consistent feature nor is it easy to distinguish it from noise in the density measurement. This lack of consistent density structure correlated with the peak magnetic field is in contrast with the development of small-scale flux ropes at Venus [*Elphic and Russell*, 1983], where axial density cavities tend to occur in association with flux ropes at high altitudes and the field strengths tend to increase with decreasing altitude.

[25] The ground tracks of the flux ropes detected in our survey are shown in Figure 11. In Figure 11 the color coding represents the peak magnetic field strength. The ground tracks of the selected flux ropes cluster around the strong crustal arcades in the Martian southern hemisphere. This result is in sharp contrast to the results of the study by *Vignes et al.* [2004] in which small-scale flux ropes were detected only in the Martian northern hemisphere, away from most strong crustal fields.

[26] We now give some statistical results from this survey, using the $B_{\mathrm{Peak}}/\sqrt{2}$ range to define the boundaries. The peak B field strength for the events was between 18 and 129 nT with a median of 60 nT. As a multiple of the crustal field at the time of the peak magnetic field measurement, the peak field strength ranged from a factor of 5 to 19 with a median of 9. The altitude at peak field was between 279 and 1120 km with a median of 338 km, a result that must be biased upward by sampling near periapsis. Solar zenith angles of peak field were from 8° to 93° with a median of 40°. Finally, the measured horizontal extent of the flux rope, as roughly determined by the time interval times 4 km/s (the approximate spacecraft velocity at periapsis), ranges between 272 and 1267 km with a median of 694 km. This result is, again, biased upward by our resolution limit of ~120 km.

[27] Finally, we note that the values for the two events analyzed in section 4 have B_{Peak} values of 90 and 55 nT at 15 and 11 times the crustal value, peak-B-field altitudes of 283 and 298 km, and horizontal extent measurements of 664 and 694 km. Because the path of MARSIS is nearly normal to the flux rope axis in both cases, the horizontal extent of each of these two events is a good estimate of the actual diameter of the flux rope. Both values are very close to the median of measured horizontal extent.

7. Discussion and Conclusion

[28] We have detected two large magnetic enhancements in the Martian ionosphere with two spacecraft in near coincidence. Minimum variance analysis on these two events shows that the magnetic field rotates in a way characteristic of a flux rope. The intermediate variance axis gives us the axis of the flux rope. The peak magnetic fields are aligned along the direction of the computed axis. We conclude that these structures are flux ropes, quasi-stable for at least a half hour. The diameter of these structures is between 650 and 700 km. These structures are directly downstream of strong crustal magnetic fields.

[29] We have detected numerous other large-scale magnetic flux ropes in the Martian ionosphere. These flux ropes have diameters of hundreds of kilometers and occur in the vicinity of strong crustal field structures.

[30] All of the flux ropes detected at Mars up through the survey by *Vignes et al.* [2004] are of the small-scale or filamentary type, with diameters of a few tens of kilometers. Because Mars Express collects an ionogram every 7.5 s and its speed at periapsis is ~4 km/s, the smallest structure detectable by MARSIS is ~120 km in diameter. Small-scale flux ropes are therefore virtually invisible to MARSIS. The large-scale flux ropes first seen at Mars by *Brain et al.* [2010] and confirmed in this paper differ from small-scale flux ropes in that they are much larger, tend to have greater peak magnetic field strength, and are located near rather than away from strong magnetic fields. The large-scale flux ropes reported by *Brain et al.* [2010] and the two cases analyzed in section 4 are all near the Martian south pole, directly downstream of the strong crustal field arcades. Figure 11 shows that the 15 cases identified in our survey are tightly clustered around these arcades. These characteristics imply that large-scale flux ropes are fundamentally different from the small-scale, filamentary, flux ropes re-

Figure 10. Magnetic field strength and density of 15 selected magnetic flux ropes. Time is centered on the universal time of the peak magnetic field strength for each selected flux rope. The magnetic field strength measured using MARSIS electron cyclotron echoes is shown in black. The electron density, normalized so that the maximum is 1, is shown in red. The electron density divided by a simple density model and normalized to a maximum of 1 is shown in blue. The traces are given in ascending order of altitude of the peak magnetic field strength so that Figures 10a–10c give the five flux rope detections at lowest, middle, and highest values of altitude of the peak magnetic field, respectively.

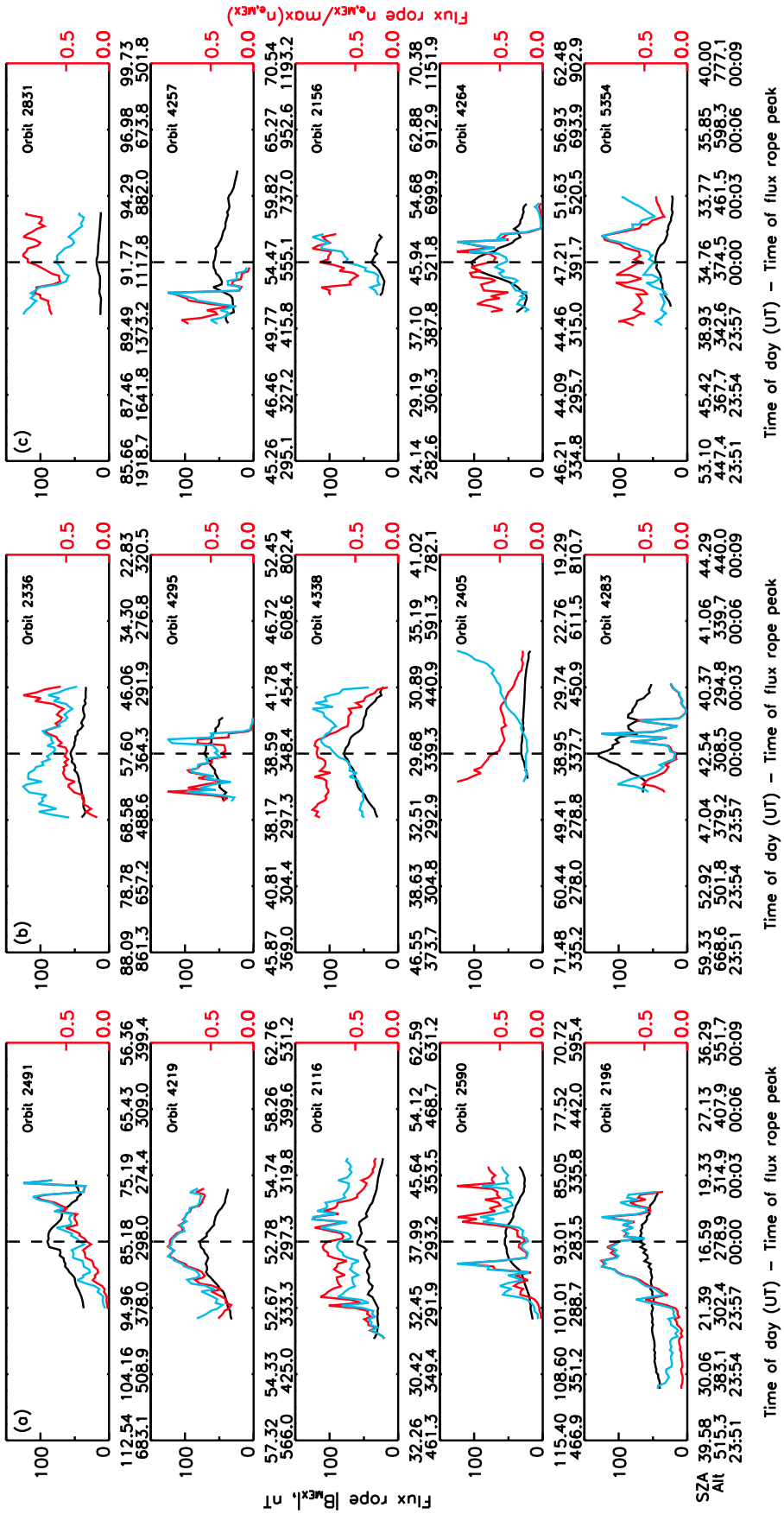
(a)
(b)
(c)
Orbit 2491
Orbit 2336
Orbit 2831
Orbit 4219
Orbit 4295
Orbit 4257
Orbit 2116
Orbit 4338
Orbit 2156
Orbit 2590
Orbit 2405
Orbit 4264
Orbit 2196
Orbit 4283
Orbit 5354
Flux rope |B_MEX|, nT
Flux rope n_e,MEX/max(n_e,MEX)
Time of day (UT) – Time of flux rope peak
SZA
Alt

Figure 10

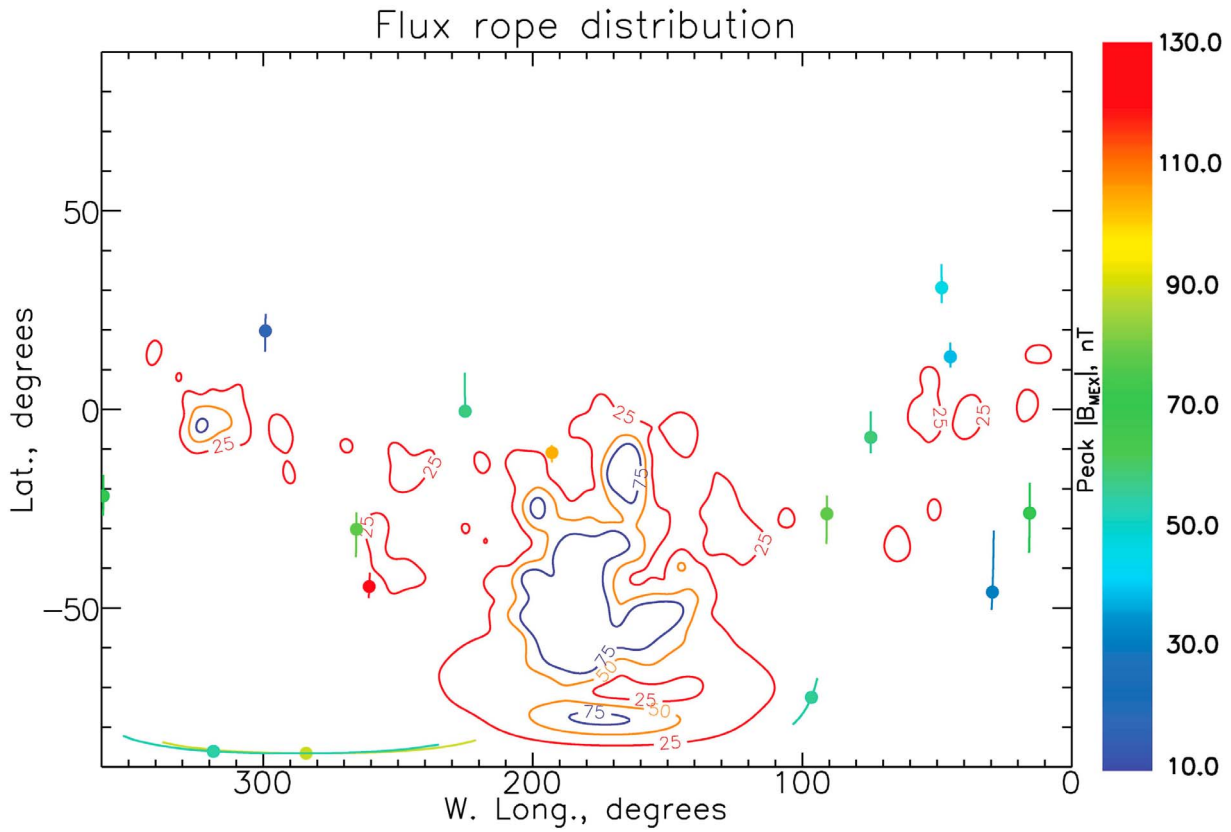

Figure 11. Ground tracks of flux ropes detected by MARSIS. The tracks are mapped according to west longitude (horizontal axis) and latitude (vertical axis). The color indicates peak magnetic field strength according to the color bar.

ported at Mars by *Cloutier et al.* [1999] and *Vignes et al.* [2004].

[31] The decreases in electron flux seen in both the MGS ER data and the MEX ASPERA-3 ELS data are probably due to field-elongated ionospheric electron distributions rotating with the magnetic field and being missed by the detector. They are indicative of field rotation but tell us nothing of a generation mechanism. The plasma contained in these flux ropes appears to be ionospheric, detected at some distance above the region of ionization.

[32] Martian flux ropes have been modeled on two occasions. The nightside flux rope associated with signatures of magnetic reconnection reported by *Eastwood et al.* [2008] was modeled using a particle-in-cell simulation. This flux rope was observed downstream of the Martian southern hemisphere crustal fields, although its association with those fields may be coincidental. This simulation, coupled with MGS MAG/ER data, clearly showed a magnetic reconnection signature. The apparent size of this flux rope, about 50 km, indicates that this may be a large example of a small-scale flux rope.

[33] Multifluid simulations of flux rope generation at terminator crossings of crustal field structures have been presented by *Harnett* [2009]. Her simulation generated a near-terminator flux rope of ~1250 km diameter and axial magnetic field strength of ~100 nT that was convected downstream away from the planet at 20 to 40 km/s at altitudes of 2300–7500 km. The simulated flux rope becomes larger as the magnetic field dissipates on a timescale of several minutes. Both of these simulations also generate a plasma density increase rather than a dropout in the interior of the flux rope, unlike some high-altitude observations of small-scale flux ropes [*Elphic et al.*, 1980]. The simulation by Harnett is consistent with the observation of *Brain et al.* [2010], who describe the formation of this type of flux rope as follows: magnetically trapped plasma in high-field regions in the Martian ionosphere is swept tailward through any of several possible interactions with the solar wind; as the field is stretched it reconnects, forming a flux rope, similar to the process invoked for formation of plasmoids in the Earth's magnetosphere.

[34] On the whole, our observations are consistent with this picture. Our survey of MARSIS-detected flux ropes shows a very clear association with strong crustal fields at southern and midlatitudes. Our observation of a quasi-stable flux rope at an altitude of ~300 km over periods of a half hour differs sharply from Harnett's simulated flux rope at much higher altitudes with a lifetime of 3 min. The high altitudes derived from Harnett's simulation imply higher velocities and stronger shearing than at the lower altitudes where MARSIS can detect the magnetic field, so that shorter flux rope lifetimes should be expected. The MARSIS measurements may also reflect the quasi-stability of a dynamic process of field stretching possibly followed by reconnection rather than the observation of a single stationary flux rope. *Lundin et al.* [2006] report aurorallike

inverted Vs at Mars possibly associated with flux rope formation that exist on half hour timescales.

[35] We note here that the particle data from both MEX and MGS show no indication of reconnection. This may be because the dayside ionospheric plasma that is so conspicuous in these data overpowers any possible reconnection signature, or that the spacecraft is not magnetically connected to the reconnection site, or that the nonspinning nature of the spacecraft allows the electrons energized by reconnection to fall between detectors. It is also possible that reconnection does not occur. We leave the question of whether reconnection occurs open. What is necessary to form a flux rope is shearing of magnetized plasma, which is clearly indicated by the magnetometer measurements presented in section 4.

[36] The stretching and shearing of crustal magnetic fields is in sharp contrast to the mechanism for producing small-scale flux ropes, in which a flux tube of magnetosheath plasma penetrates the ionopause due to the curvature force overbalancing the buoyant force of the flux tube and is then rolled up into a flux rope by solar wind velocity shearing [see *Russell*, 1990]. *Wei et al.* [2010] note that this shearing process is suppressed by the presence of strong ambient magnetic fields such as the crustal fields of Mars.

[37] The clear dichotomy between the two types of flux rope is somewhat obscured by the discovery of the flux rope at Titan by *Wei et al.* [2010]: the flux rope is large enough to be considered "large scale" and yet Titan has no planetary- or crustal-scale magnetic fields that would facilitate the large-scale mechanism described here. Titan's submagnetosonic immersion in the magnetic field of Saturn [*Wei et al.*, 2010] may have effects on the scaling of shear-generated flux ropes with which we are as yet unfamiliar. The absence of large-scale flux ropes at Venus reinforces the conclusion that large- and small-scale flux ropes are distinct types.

[38] The question remains as to whether these large-scale flux ropes are force free, e.g., dominated by magnetic rather than plasma pressure. *Elphic et al.* [1980] speculates that small-scale flux ropes become more force free as they evolve downward in altitude. The electron density plots in Figure 10b are inconclusive on this point. Orbits 2590, 2118, 2491, 4283, 4295, 2336, 5354, and 4264 all look like they might have a depression in plasma density near the magnetic field peak, but the dropouts are not large enough to clearly distinguish them from general density fluctuations. Even if these density dropouts are real, there is still no differentiation with altitude. *Harnett* [2009] and *Brain et al.* [2010] describe an increase in plasma density near the flux rope axis, implying a non-force-free, nonequilibrium situation.

[39] We conclude that we have detected large-scale flux ropes at Mars using the MARSIS ionospheric sounding receiver. The large-scale flux ropes that are the subject of this study are different from the small-scale, or filamentary, flux ropes that have previously been studied at Mars and Venus. The distinctions between the two types of flux rope are as follows.

[40] 1. The diameters of small-scale flux ropes at Mars and Venus is on the order of a few tens of kilometers, while those of large-scale flux ropes are several hundred to over a thousand kilometers.

[41] 2. The peak magnetic field strengths of small-scale flux ropes at Mars reach a maximum of about 20 nT, while those of large-scale flux ropes at Mars have been seen almost as high as 200 nT.

[42] 3. Small-scale flux ropes appear to be suppressed by the presence of strong magnetic fields, such as the Martian crustal fields, while large-scale flux ropes cluster around the strong crustal fields in the southern hemisphere of Mars.

[43] **Acknowledgments.** This research was supported by NASA through contract 1224107 with the Jet Propulsion Laboratory and contract NASW-00003 at Southwest Research Institute.

[44] Masaki Fujimoto thanks Peter Israelevich and another reviewer for their assistance in evaluating this paper.

References

Acuña, M. H., et al. (2001), Magnetic field of Mars: Summary of results from the aerobraking and mapping orbits, *J. Geophys. Res.*, *106*, 23,403–23,417, doi:10.1029/2000JE001404.

Akalin, F., D. D. Morgan, D. A. Gurnett, D. L. Kirchner, D. A. Brain, R. Modolo, M. H. Acuña, and J. R. Espley (2010), Dayside induced magnetic field in the ionosphere of Mars, *Icarus*, *206*, 104–111, doi:10.1016/j.icarus.2009.03.021.

Barabash, S., et al. (2004), ASPERA-3: Analyser of Space Plasmas and Energetic Ions for Mars Express, in *Mars Express: A European Mission to the Red Planet*, edited by A. Wilson, pp. 121–140, Eur. Space Agency Publ. Div., Noordwijk, Neth.

Brain, D. A., F. Bagenal, M. H. Acuña, and J. E. P. Connerney (2003), Martian magnetic morphology: Contributions from the solar wind and crust, *J. Geophys. Res.*, *108*(A12), 1424, doi:10.1029/2002JA009482.

Brain, D. A, A. H. Baker, J. Briggs, J. P. Eastwood, J. S. Halekas, and T.-D. Phan (2010), Episodic detachment of Martian crustal magnetic fields leading to bulk atmospheric escape, *Geophys. Res. Lett.*, *37*, L14108, doi:10.1029/2010GL043916.

Browning, P. K. (1990), Twisted flux ropes in the solar corona, in *Physics of Magnetic Flux Ropes*, *Geophys. Monogr. Ser.*, vol. 58, edited by C. T. Russell, E. R. Priest, and L. C. Lee, pp. 219–228, AGU, Washington, D. C.

Cain, J. C., B. B. Ferguson, and D. Mozzoni (2003), An $n = 90$ internal potential function of the Martian crustal magnetic field, *J. Geophys. Res.*, *108*(E2), 5008, doi:10.1029/2000JE001487.

Chicarro, A., P. Martin, and R. Trautner (2004), The Mars Express mission: An overview, in *Mars Express: A European Mission to the Red Planet*, edited by A. Wilson, pp. 3–16, Eur. Space Agency Publ. Div., Noordwijk, Neth.

Cloutier, P. A., et al. (1999), Venus-like interaction of the solar wind with Mars, *Geophys. Res. Lett.*, *26*, 2685–2688.

Cravens, T. E., H. Shinagawa, and J. G. Luhmann (1997), Magnetohydrodynamic processes: Magnetic fields in the ionosphere of Venus, in *Venus II*, edited by S. W. Bougher, D. M. Hunten, and R. J. Phillips, pp. 61–93, Univ. of Ariz. Press, Tucson, Ariz.

Duru, F., D. A. Gurnett, D. D. Morgan, R. Modolo, A. F. Nagy, and D. Najib (2008), Electron densities in the upper ionosphere of Mars from the excitation of electron plasma oscillations, *J. Geophys. Res.*, *113*, A07302, doi:10.1029/2008JA013073.

Eastwood, J. P., D. A. Brain, J. S. Halekas, J. F. Drake, T. D. Phan, M. Øieroset, D. L. Mitchell, R. P. Lin, and M. Acuña (2008), Evidence for collisionless magnetic reconnection at Mars, *Geophys. Res. Lett.*, *35*, L02106, doi:10.1029/2007GL032289.

Elphic, R. C., and C. T. Russell (1983), Magnetic flux ropes in the Venus ionosphere: Observations and models, *J. Geophys. Res.*, *88*, 58–72, doi:10.1029/1983JA088iA01p00058.

Elphic, R. C., C. T. Russell, J. A. Slavin, and L. H. Brace (1980), Observations of the dayside ionopause and ionosphere of Venus, *J. Geophys. Res.*, *85*, 7679–7696, doi:10.1029/1980JA085iA13p07679.

Gurnett, D. A., et al. (2005), Radar soundings of the ionosphere of Mars, *Science*, *310*, 1929–1933.

Harnett, E. M. (2009), High-resolution multifluid simulations of flux ropes in the Martian magnetosphere, *J. Geophys. Res.*, *114*, A01208, doi:10.1029/2008JA013648.

Hesse, M., and M. G. Kivelson (1998), The formation and structure of flux ropes in the magnetotail, in *New Perspectives on the Earth's Magnetotail*, *Geophys. Monogr. Ser.*, vol. 105, edited by A. Nishida, D. N. Baker, and S. W. H. Cowley, pp. 139–151, AGU, Washington, D. C.

Hones, E. W., Jr., D. N. Baker, S. J. Bame, W. C. Feldman, J. T. Gosling, D. J. McComas, R. D. Zwickl, J. A. Slavin, E. J. Smith, and B. T. Tsurutani (1984a), Structure of the magnetotail at 220 R_e and its response to geo-

magnetic activity, *Geophys. Res. Lett.*, *11*, 5–7, doi:10.1029/GL011i006p00599.

Hones, E. W., Jr., J. Birn, D. N. Baker, S. J. Bame, W. C. Feldman, D. J. McComas, and R. D. Zwickl (1984b), Detailed examination of a plasmoid in the distant magnetotail with ISEE 3, *Geophys. Res. Lett.*, *11*, 1046–1049, doi:10.1029/GL011i010p01046.

Jordan, R., et al. (2009), The Mars Express MARSIS sounder instrument, *Planet. Space Sci.*, *57*, 1975–1986, doi:10.1016/j.pss.2009.09.016.

Lepping, R. P., J. A. Jones, and L. F. Burlaga (1990), Magnetic field structure of interplanetary magnetic clouds at 1 AU, *J. Geophys. Res.*, *95*, 11,957–11,965.

Lundin, R., et al. (2006), Auroral plasma acceleration above Martian magnetic anomalies, *Space Sci. Rev.*, *126*, 333–354, doi:10.1007/s11214-006-9086-x.

Lundin, R., S. Barabash, M. Holmström, H. Nilsson, M. Yamauchi, M. Fraenz, and E. M. Dubinin (2008), A comet-like escape of ionospheric plasma from Mars, *Geophys. Res. Lett.*, *35*, L18203, doi:10.1029/2008GL034811.

Mitchell, D. L., R. P. Lin, C. Mazelle, H. Réme, P. A. Cloutier, J. E. P. Connerney, M. H. Acuña, and N. F. Ness (2001), Probing Mars' crustal magnetic field and ionosphere with the MGS Electron Reflectometer, *J. Geophys. Res.*, *106*, 23,419–23,427.

Morgan, D. D., D. A. Gurnett, D. L. Kirchner, J. L. Fox, E. Nielsen, and J. J. Plaut (2008), Variation of the Martian ionospheric electron density from Mars Express radar soundings, *J. Geophys. Res.*, *113*, A09303, doi:10.1029/2008JA013313.

Picardi, G., et al. (2004), MARSIS: Mars Advanced Radar for Subsurface and Ionosphere Sounding, in *Mars Express: A European Mission to the Red Planet*, edited by A. Wilson, pp. 1–19, Eur. Space Agency Publ. Div., Noordwijk, Neth.

Priest, E. R. (1990), The equilibrium of magnetic flux ropes, in *Physics of Magnetic Flux Ropes*, *Geophys. Monogr. Ser.*, vol. 58, edited by C. T. Russell, E. R. Priest, and L. C. Lee, pp. 1–22, AGU, Washington, D. C.

Russell, C. T. (1990), Magnetic flux ropes in the ionosphere of Venus, in *Physics of Magnetic Flux Ropes*, *Geophys. Monogr. Ser.*, vol. 58, edited by C. T. Russell, E. R. Priest, and L. C. Lee, pp. 413–423, AGU, Washington, D. C.

Russell, C. T., and R. C. Elphic (1979), Observation of magnetic flux ropes in the Venus ionosphere, *Nature*, *279*, 616–618.

Slavin, J. A., R. P. Lepping, J. Gjerloev, D. H. Fairfield, M. Hesse, C. J. Owen, M. B. Moldwin, T. Nagai, A. Ieda, and T. Mukai (2003), Geotail observations of magnetic flux ropes in the plasma sheet, *J. Geophys. Res.*, *108*(A1), 1015, doi:10.1029/2002JA009557.

Slavin, J. A., et al. (2009), MESSENGER observations of magnetic reconnection in Mercury's magnetosphere, *Science*, *324*, 606–610, doi:10.1126/science.1172011.

Sonnerup, B. U. Ö., and L. J. Cahill Jr. (1968), Explorer 12 observations of the magnetopause current layer, *J. Geophys. Res.*, *73*, 1757–1770, doi:10.1029/JA073i005p01757.

Vignes, D., M. H. Acuña, J. E. P. Connerney, D. H. Crider, H. Rème, and C. Mazelle (2004), Magnetic flux ropes in the Martian atmosphere: Global characteristics, *Space Sci. Rev.*, *111*, 223–231.

Wei, H. Y., C. T. Russell, T. L. Zhang, and M. K. Dougherty (2010), Comparison study of magnetic flux ropes in the ionospheres of Venus, Mars and Titan, *Icarus*, *206*, 174–181, doi:10.1016/j.icarus.2009.03.14.014.

F. Akalin, F. Duru, D. A. Gurnett, J. S. Leisner, and D. D. Morgan, Department of Physics and Astronomy, University of Iowa, 718 Van Allen Hall, Iowa City, IA 52242, USA. (ferzan-akalin@uiowa.edu; firdevs-duru@uiowa.edu; donald-gurnett@uiowa.edu; jared-leisner@uiowa.edu; david-morgan@uiowa.edu)

D. A. Brain, Space Physics Research Group, Space Sciences Laboratory, University of California, Berkeley, CA 94720, USA. (brain@ssl.berkeley.edu)

R. A. Frahm and J. D. Winningham, Southwest Research Institute, PO Drawer 28510, San Antonio, TX 78228, USA. (rfrahm@swri.edu; dwinningham@mac.com)